Study on high-accuracy orientation with lunar remote sensing imagery

ZHANG Jixian[1], DENG Kazhong[2], CHENG Chunquan[1,2], YAN Qin[1], NING Xiaogang[1], GUO Jian[1]

1. *Chinese Academy of Surveying and Mapping, Beijing* 100830, *China*;
2. *China University of Mining & Technology, Jiangsu Xuzhou* 221116, *China*

Abstract: High-accuracy 3D image positioning is considered as the foundation of lunar topographic mapping. This study simulated the influence on image positioning from errors and correlations of Chang'e-1 optical sensor orientation elements, and established the rigorous block adjustment model suitable for lunar optical remote sensing images. The errors and area limits caused by the lunar curvature were avoided in this model established under the Selenocentric Orthogonal Coordinate System (SOCS), the accidental errors of exterior line elements were reduced by orbit fitting and interpolation, the polynomial orders of systematic errors in satellite orbits were decreased with their expression in the flying coordinate system moving and rotating with satellites, and the reliability of exterior orientation solution was enhanced under the condition of sparse and low accuracy control points by appending constraint of orbit and attitude parameters. Finally, 60 scenes of Clementine images near the south pole of the Moon were utilized in 10 strips with the area of around 195000km^2 and ULCN2005 GCPs as the experimental data, and a series of helpful results was achieved on image positioning of the Moon.

Key words: rigorous model, image orientation, lunar mapping, error simulation

CLC number: P236 **Document code:** A

Citation format: Zhang J X, Deng K Z,Cheng C Q, Yan Q, Ning X G and Guo J. 2010. Study on high-accuracy orientation with lunar remote sensing imagery. *Journal of Remote Sensing.* **14**(3): 423—436

1 INTRODUCTION

The Moon is the nearest planet of the Earth, and lunar exploration has been a hot research field all around the world. Topographic mapping on the Moon is the primary task of Chang'e-1 (CE-1) satellite, which was launched in 2007 as China's first lunar exploration satellite. Based on optical remote sensing images as the major data source at present, image matching and high-accuracy image positioning are vital for lunar topographic mapping.

With the topographic shapes and figures, the lunar topographic mapping based on optical image is quite different from that of the Earth. The remote sensing images on earth are mostly adopted as the default data source in the current commercial remote sensing image processing software, which is not convenient and suitable to process lunar images because of the utilization of the parameters of the Earth in the system. Though Wang (2008a; 2008b) has analyzed the photogrammetry accuracy of CE-1 optical sensor and aero-triangulation of images with 1/4 orbit long flight strips, the research on lunar image orientation still remains limited in China.

2 COLLINEAR EQUATION OF OPTICAL IMAGERY IN SOCS

For aerial photogrammetry in a small range, the object coordinate system is often established on tangent sphere orthogonal coordinate system of the Earth (Moon) or the corresponding orthogonal coordinate system at a basis of the projected plane. Due to the influence of the Earth (Moon) curvature, the values and even the signs of exterior orientation elements will change with the increasing length of flight strips, when photogrammetry is processed in the tangent sphere rectangular coordinate system. Therefore, it is a common approach to divide the flight strip into subsections and adjust the seriatim (Wang *et al.*, 2008a; Wang, 1979). The ellipsoidal surface, when projected to a plane, will result in distortion, and the projective distortion on the Moon will be more remarkable than that on the Earth be cause of its shorter radius. Taking testing data as an example in this study, the distance from the edge of image to the tangent plane or projected plane will be more than 25km even if the origin is set at the center of these images for the tangent sphere rectangular coordinate system or the projective center. Transforma-

Received: 2009-02-24; **Accepted**: 2009-04-01

Foundation: National Natural Science Foundation of China (No:40871167 and No: 40801192).

First author biography: ZHANG Jixian(1965—), male, professor, supervisor of doctoral candidates the president of Chinese Academy of Surveying and mapping. His research interests include photogrammetry and remote sensing, geographical information system, and integration and application of RS, GIS and GPS. E-mail: zhangjx@ casm.ac.cn

tion between different coordinate systems can be reduced in the geocentric coordinate system for multi-source data processing, which is suitable for combining processing of large-area images. Image positioning of spaceborne photos on earth has been transferred into the geocentric coordinate system gradually. The orientation model of the linear array sensor image can be formed as follows (Kratky, 1989; Yuan, 2003):

$$\begin{bmatrix} x \\ 0 \\ -f \end{bmatrix} = \lambda M^{-1} \begin{bmatrix} X - X_s \\ Y - Y_s \\ Z - Z_s \end{bmatrix} \tag{1}$$

Where (x,y) is the coordinate in the image coordinate system, f is the focus of the camera, (X_s, Y_s, Z_s), (X, Y, Z) are coordinates of the sensor center and the ground object point in the geocentric coordinate system respectively, $\boldsymbol{M}$ expresses the rotation matrix of satellite attitudes and orbit parameters.

Similar to triangulation of remote sensing imagery in the geocentric orthogonal coordinate system, positioning of the Moon remote sensing imagery will be implemented in the selenocentric orthogonal coordinate system. And the similar orientation model will be adopted. Set

$\boldsymbol{M} = \boldsymbol{R}_o^{\ E} \cdot \boldsymbol{R}_b^{\ o} \cdot \boldsymbol{R}_c^{\ b} = [m_{ij}]$, i,j=1,2,3. m_{ij} expresses elements in matrix $\boldsymbol{M}$.

Where $\boldsymbol{R}_o^{\ E}$, $\boldsymbol{R}_b^{\ o}$ and $\boldsymbol{R}_c^{\ b}$ denote the transformations from the orbit coordinate system to the selenocentric orthogonal coordinate system, from the body coordinate system to the orbit coordinate system, from the sensor coordinate system to the body coordinate system, respectively, which are the functions of satellite state vectors, attitudes and mounting angles of the sensor.

Testing data for block adjustment will be area array CCD sensor images in this study; after changing $[x, 0, -f]^{\mathrm{T}}$ at the left of Eq. (1) into $[x-x_0, y-y_0, -f]^{\mathrm{T}}$, collinear equations will be shown as follows:

$$\begin{cases} x - x_0 = -f \dfrac{m_{11}(X - X_s) + m_{21}(Y - Y_s) + m_{31}(Z - Z_s)}{m_{13}(X - X_s) + m_{23}(Y - Y_s) + m_{33}(Z - Z_s)} \\ y - y_0 = -f \dfrac{m_{12}(X - X_s) + m_{22}(Y - Y_s) + m_{32}(Z - Z_s)}{m_{13}(X - X_s) + m_{23}(Y - Y_s) + m_{33}(Z - Z_s)} \end{cases} \tag{2}$$

Because the transformation matrix from the selenocentric orthogonal coordinate system to the geocentric orthogonal coordinate system is the function of satellite state vectors, its accuracy will be fined gradually during the adjustment process. The transformation matrix from the sensor coordinate system to the body coordinate system is acquired from calibration parameters when the camera is calibrated. It is usually accurate and highly correlated with exterior orientation parameters; therefore, its effect on imagery positioning can be decreased by correcting the orientation parameters. Thereby, the interior, exterior orientation parameters and coordinate of the object on the moon surface can be selected as adjustment unknowns, and the normal forms of linearized error equations will be (Wang, 1979):

$$\begin{cases} v_x = (x) - x + f_{11}\Delta X_s + f_{12}\Delta Y_s + f_{13}\Delta Z_s + \\ \quad f_{14}\Delta\omega + f_{15}\Delta\varphi + f_{16}\Delta\kappa + f_{17}\Delta f + \\ \quad f_{18}\Delta x_0 - f_{11}\Delta X - f_{12}\Delta Y - f_{13}\Delta Z \\ v_y = (y) - y + f_{21}\Delta X_s + f_{22}\Delta Y_s + f_{23}\Delta Z_s + \\ \quad f_{24}\Delta\omega + f_{25}\Delta\varphi + f_{26}\Delta\kappa + f_{27}\Delta f + \\ \quad f_{29}\Delta y_0 - f_{21}\Delta X - f_{22}\Delta Y - f_{23}\Delta Z \end{cases} \tag{3}$$

where f_{ij}(i=1,2, j=1,2,…,8) denotes coefficients of error equations after linearization, (x) and (y) express image coordinate computing values of point on the ground according to orientation parameters, x and y are coordinate measurement values of point on image, ΔX_s, ΔY_s, ΔZ_s, $\Delta\omega$, $\Delta\varphi$ and $\Delta\kappa$ express corrections of exterior orientation parameters, Δx_0 and Δy_0 express corrections of interior orientation parameters, ΔX, ΔY and ΔZ denote corrections of point on the ground.

3 THE SIMULATION OF LINEAR ARRAY IMAGE ORIENTATION ERRORS OF CHANG'E-1

For the influence factor complication of image orientation errors, all of the errors can not be considered at the same time in the rigorous model. Positioning errors caused by one factor without being considered can be compensated by correcting its other correlated parameters in the model. Meanwhile, if the correlated parameters exist in the error equations, new error influence factors will be brought to reduce the stability and reliability of computation due to the incomplete correlations between unknowns. Consequently, the problems are required to be considered in the lunar image positioning model including the correlation removal of rigorous model (Zhang, 2004) and the largest errors limit of the correlated orientation parameters leading to the residuals after compensation negligible relative to the required precision of positioning. In this study, errors and correlations of orientation parameters influencing the positioning will be simulated aiming at CE-1 optical sensor.

For CE-1, the optical sensor is a three-line CCD camera in the tangent sphere coordinate system taking a point on the lunar surface corresponding to a linear array image center as the origin, the direction of linear array as X axis, and the flight direction as Y axis. The terrain of the Moon can be simulated by the sine and circularity function as follows:

$$\begin{cases} Z = \mathrm{d}H \times \sin(2\pi X / Tt) + \sqrt{R_M^2 - X^2} - R_M \\ Y = 0 \end{cases} \tag{4}$$

Where R_M denotes radius of the Moon, and X expresses the coordinate of ground point in the linear array direction.

Lunar sphere parameters are adopted as foundation in this function, and the sinuous curve is overlapped with a swing of 3km as the simulated terrain. The model can express different elevations at different locations in the range of the image. The shape of the terrain is shown in Fig. 1.

Parameters of the CE-1 optical sensor are shown as follow: focus f=23.33mm, its focal plane CCD area array is 1024×1024 pixels; left-middle-right three lines are selected to form the front-

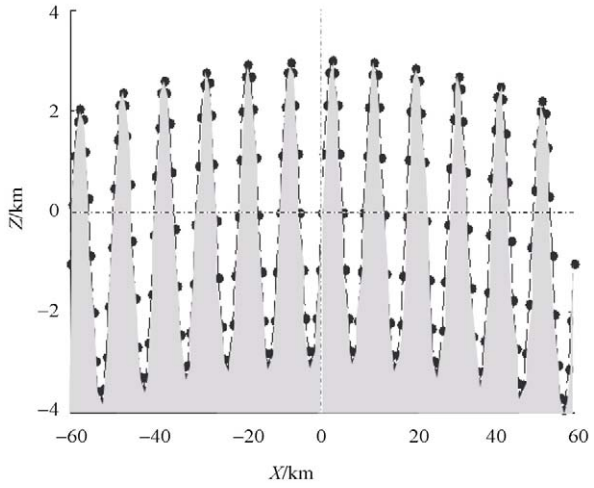

Fig. 1 Simulative terrain

nadir-back-viewing linear array, the angle of sight between linear arrays is 17° degree, intercepted line contains 512 pixels, and the size of a pixel is 14μm. The orbit is near-pole orbit with a designed height of 200km. (Wang *et al*, 2008a).

When emulating the errors of direct positioning of CE-1 satellite image, satellite project center X_s, Y_s and Z_s values add 300m as errors respectively, interior elements x_0, y_0, and f_0 values add 0.05mm as errors respectively, and satellite attitudes ω, φ and κ values add 0.1° as errors. Based on Eq. (2) and Eq. (3), the simulated terrain, CE-1 optical sensor parameters and designed orbit and parameters, CE-1 three-linear sensor nadir and backward images are adopted to emulate stereo positioning errors. Orientation parameters without errors are used to imaging, and orientation parameters with errors and the simulated images for forward intersection and stereo positioning. The simulated photograph state is shown in Fig.2. The resulted errors in the direction of array d*X*, flight direction of satellite d*Y* and height direction d*Z* curves are showed in Fig. 3. The horizontal axis *X* refers to ground point coordinates corresponding to one line image.

It can be concluded from the figure that errors of the image direct positioning are large and nearly linear to the position of pixels in the linear array, and also consistent with the variation of terrain.

In the simulation of compensation residual correlation, attitudes and focal points are adopted as unknown parameters and other orientation parameter values with errors as accurately known data; two control points on both sides of the linear image are used to calculate corrections of unknowns by Eq. (3). Then, adjusted parameters and unadjusted parameters with errors are used as orientation data for forward intersection. Fig. 4 shows the errors of one line image result in direction of array d*X*, flight direction of satellite d*Y* and height direction d*Z* curves. The horizontal axis *X* is ground point coordinates corresponding to one line image.

Due to the stability of satellite platform and parallel projection of images between different lines, the errors of orientation elements of images lines are similar near the control points and containing control points. Though direct positioning and residuals after compensation is different because of the influences from different terrains, the rule is the same, and the similar results

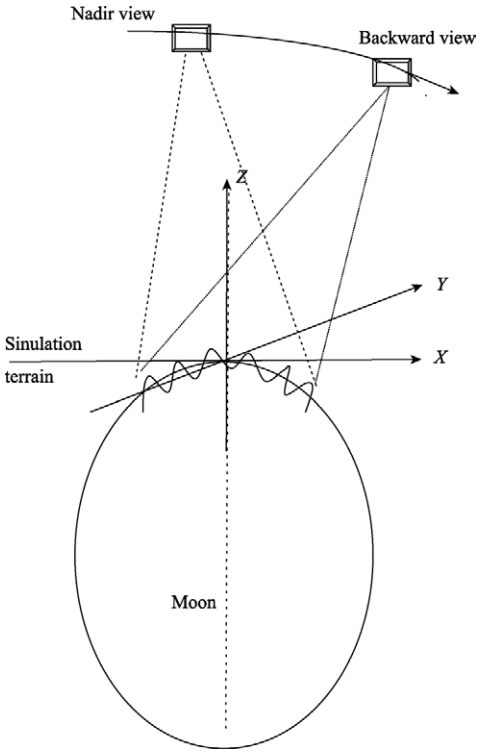

Fig. 2 Simulative photogrammetry

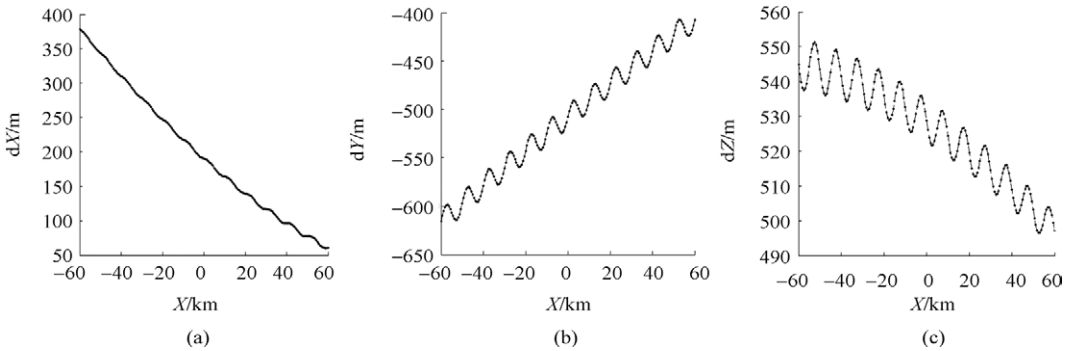

Fig. 3 Simulation of positioning errors
(a) *X* axis direction; (b) *Y* axis direction; (c) *Z* axis direction

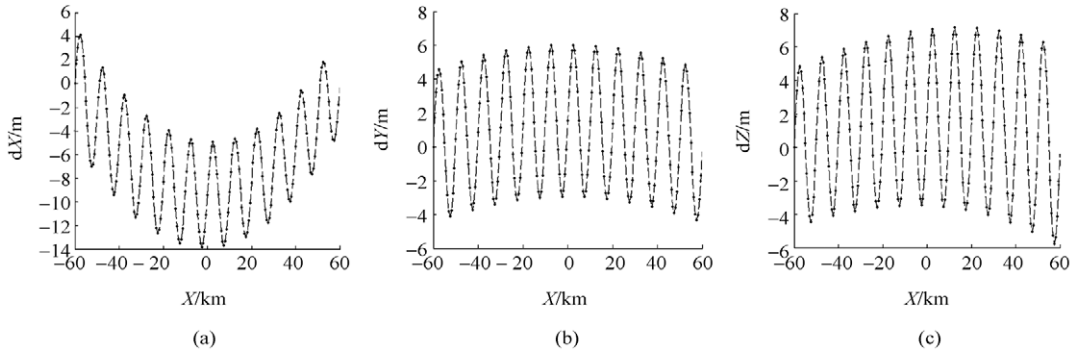

Fig. 4 Simulation of residual positioning errors corrected by correlative parameters
(a) *X* axis direction; (b) *Y* axis direction; (c) *Z* axis direction

will exist when control points are on both sides of different image lines. The results of emulation show that with control or adjustment, if the precision of satellite position is in 300m, the precision of interior orientation elements can be smaller than 0.05mm, and the maximum of residuals after compensation in three axes is smaller than 15m when attitudes and focal points are used as unknowns while others are regarded true during the positioning, which is acceptable relative to the precision of control points and the image resolution of CE-1.

4 CORRECTION MODEL FOR ORBIT

In this study, the correction model of sensor position is based on the flight coordinate system, the accidental errors of surveying ephemeris data are corrected with fitting of orbit parameters and interpolation of the satellite state vector, and systematic errors of the orbit are reduced with ground control points.

4.1 The fitting of the orbit shape and interpolation of satellite position

The aim of fitting and interpolation of orbit shape is to remove accidental errors of satellite, and make the initial position value of the same orbit to be systematic. The auxillary data of image supply discrete satellite position vectors in non-inertia coordinate system, and the orbit shape can be fitted according to these positions. Due to the influence of rotation, it is required to transform from Moon-fixed SOCS(MFSOCS), that is non-inertia SOCS, to inertia SOCS. The angle between non-inertia and inertia SOCS of the i^{th} ephemeris is supposed as θ_i, the position of satellite between these two coordinate systems is

$$\begin{bmatrix} X_{iI} & Y_{iI} & Z_{iI} \end{bmatrix}^{\mathrm{T}} = \boldsymbol{R}_3(\theta_i)[X_{iR} \quad Y_{iR} \quad Z_{iR}]^{\mathrm{T}} \tag{5}$$

$[X_{iR}\ Y_{iR}\ Z_{iR}]$ is the coordinate of MFSOCS , while $[X_{iI}\ Y_{iI}\ Z_{iI}]$ is the coordinate of inertia SOCS.

In the inertia coordinate system, the relation ship between six orbit parameters a, e, I, Ω, ω, f and three-dimension coordinate system is:

$$\begin{cases} X_{iI} = r(\cos\Omega\cos u - \sin\Omega\sin u_i\cos i) \\ Y_{iI} = r(\sin\Omega\cos u + \cos\Omega\sin u_i\cos i) \\ Z_{iI} = r\sin u_i\sin i \end{cases} \tag{6}$$

where: $r = \dfrac{a(1-\mathrm{e}^2)}{1+\mathrm{e}\cos f}$, $\quad u_i = \omega + f_i$

Based on Eq. (5) and Eq. (6), if several satellite positions and corresponding time are provided, orbit parameters in inertia selenocentric orthogonal coordinate system can be fitted by least squares, and positions and velocity vectors of any time can be interpolated according to these orbit parameters.

4.2 Flight coordinate system and orbit correction model

In the flight coordinate system, the direction of axis *X* is the vector direction of satellite velocity, axis *Y* is perpendicular to the plane composed of the position and velocity vectors, and axis *Z* is determined by the right-hand rule. O_1-$X_1Y_1Z_1$ and O_2-$X_2Y_2Z_2$ are shown in Fig. 5 as an example. The mathematic expression of three axes of this coordinate system is:

$$\begin{cases} \boldsymbol{X}_v = [(X_v)_X, (X_v)_Y, (X_v)_Z] = \boldsymbol{V}(t)/\|\boldsymbol{V}(t)\| \\ \boldsymbol{Y}_v = [(Y_v)_X, (Y_v)_Y, (Y_v)_Z] = [\boldsymbol{P}(t)\times\boldsymbol{V}(t)]/\|\boldsymbol{P}(t)\times\boldsymbol{V}(t)\| \\ \boldsymbol{Z}_v = [(Z_v)_X, (Z_v)_Y, (Z_v)_Z] = \boldsymbol{X}_v\times\boldsymbol{Y}_v \end{cases} \tag{7}$$

Where, $\boldsymbol{P}(t_i)$ and $\boldsymbol{V}(t_i)$ are the position and velocity vectors in the selenocentric orthogonal coordinate system.

Consequently, when the position of satellite is in MFSOCS, the rotation matrix from flight coordinate system to MFSOCS is:

$$R_V E = \begin{bmatrix} (X_v)_X & (Y_v)_X & (Z_v)_X \\ (X_v)_Y & (Y_v)_Y & (Z_v)_Y \\ (X_v)_Z & (Y_v)_Z & (Z_v)_Z \end{bmatrix} \tag{8}$$

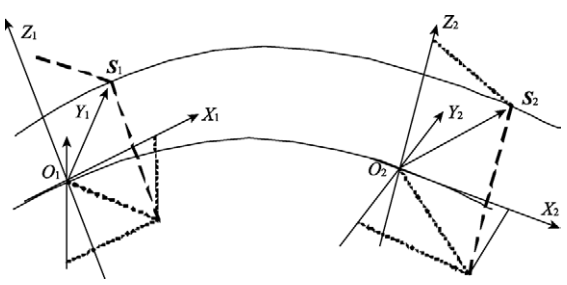

Fig. 5 System errors of orbit

The linear function or low order polynomial in three axes of the flight coordinate system is adopted in the orbit correction model.

$$\begin{cases} \Delta X_V = a_0 + a_1 t + \cdots \\ \Delta Y_V = b_0 + b_1 t + \cdots \\ \Delta Z_V = c_0 + c_1 t + \cdots \end{cases} \tag{9}$$

a_i, b_i and c_i (i=0,1…, n) are coefficients of polynomial, and t is the relative time of imaging time.

Though the orbit of satellite in selenocentric orthogonal coordinate system is required to be expressed by high-order polynomial in a short time, the orbit of satellite in a certain time is relatively stable and the error of orbit is obviously systematic. Because the flight coordinate system moves and rotates with satellite in orbit, the variation of orbit error in the flight coordinate system is slow. For example, the synchro-system error of orbit control clock is the main factor of orbit error (Giannone, 2006), and the projections of orbit error into Selenocentric Coordinate System are varying curves, however, it shows a constant in X direction of the flight coordinate. It is shown in Fig. 5 that correction vectors $\boldsymbol{O}_1\boldsymbol{S}_1$ and $\boldsymbol{O}_2\boldsymbol{S}_2$ on different station positions O_1 and O_2 show similar sizes and directions in flight coordinates O_1-$X_1Y_1Z_1$ and O_2-$X_2Y_2Z_2$. The error curve is more simple or lower in varying frequency, the order of polynomial is lower and the numbers of orientation parameters is less when polynomial fitting, thus the reliability of parameter solving could be improved under the conditions of less control points and low accuracy.

5 THE RIGOROUS ORIENTATION MODEL OF SPACEBORNE AREA ARRAY IMAGE

5.1 The coefficients of coordinate increments of station positions in flight coordinate system

In Eq. (3), the coefficients of error equations f_{11}, f_{12}, f_{13}, f_{21}, f_{22} and f_{23} are corresponding to unknown parameters of satellite positions in the selenocentric orthogonal coordinate system. It is required to convert Eq. (3) into an error formula including orbit correction model parameters in the flight coordinate system. Because the data sources of adjustment are Clementine optical area CCD sensor images, two kinds of error equations exist according to different selection of unknowns.

If a set of correction unknowns of exterior elements exist in every scene, the error equation is

$$\begin{cases} v_x = (x) - x + f_{a01}\Delta X_{Vs} + f_{b01}\Delta Y_{Vs} + f_{c01}\Delta Z_{Vs} + \\ \quad f_{14}\Delta\omega + f_{15}\Delta\varphi + f_{16}\Delta\kappa + f_{17}\Delta f + \\ \quad f_{18}\Delta x_0 - f_{11}\Delta X - f_{12}\Delta Y - f_{13}\Delta Z \\ v_y = (y) - y + f_{a02}\Delta X_{Vs} + f_{b02}\Delta X_{Vs} + f_{c02}\Delta X_{Vs} + \\ \quad f_{24}\Delta\omega + f_{25}\Delta\varphi + f_{26}\Delta\kappa + f_{27}\Delta f + \\ \quad f_{29}\Delta y_0 - f_{21}\Delta X - f_{22}\Delta Y - f_{23}\Delta Z \end{cases} \tag{10}$$

In the above equation, the increment unknowns of satellite positions are expressed by Eq. (9).

If a set of same orbit correction model parameters are used in all scenes with the same orbit section and a set of attitude increments as unknowns are adopted in every scene, the error equation is

$$\begin{cases} v_x = (x) - x + \sum_{i=0}^{n} f_{ai1}a_i + \sum_{i=0}^{n} f_{bi1}b_i + \sum_{i=0}^{n} f_{ci1}c_i + \\ \quad f_{14}\Delta\omega + f_{15}\Delta\varphi + f_{16}\Delta\kappa + f_{17}\Delta f + \\ \quad f_{18}\Delta x_0 - f_{11}\Delta X - f_{12}\Delta Y - f_{13}\Delta Z \\ v_y = (y) - y + \sum_{i=0}^{n} f_{ai2}a_i + \sum_{i=0}^{n} f_{bi2}b_i + \sum_{i=0}^{n} f_{ci2}c_i + \\ \quad f_{24}\Delta\omega + f_{25}\Delta\varphi + f_{26}\Delta\kappa + f_{27}\Delta f + \\ \quad f_{29}\Delta y_0 - f_{21}\Delta X - f_{22}\Delta Y - f_{23}\Delta Z \end{cases} \tag{11}$$

In the two equations above, f_{aij}, f_{bij} and f_{cij} (i=0, 1, …; j=1, 2) are coefficients of error equation corresponding to orbit correction model parameters in flight coordinate system. (x) and (y) are values calculated from initial values, and x and y are measured values of image points.

It can be found from the definition of the flight coordinate system that the coordinate transform between flight coordinate system and selenocentric orthogonal coordinate system is:

$$\begin{bmatrix} X_s & Y_s & Z_s \end{bmatrix}^{\mathrm{T}} = \begin{bmatrix} X_{s0} & Y_{s0} & Z_{s0} \end{bmatrix}^{\mathrm{T}} + R_V E \begin{bmatrix} \Delta X_{Vs} & \Delta Y_{Vs} & \Delta Z_{Vs} \end{bmatrix}^{\mathrm{T}} \tag{12}$$

Therefore, the relationship between coefficients of unknowns of correction model parameters in flight coordinate system in Eq. (11) and coefficients of error equation in selenocentric orthogonal coordinate system is shown as follow:

$$\begin{bmatrix} f_{aij} & f_{bij} & f_{cij} \end{bmatrix}^{\mathrm{T}} = R^{\mathrm{T}}{}_v E \begin{bmatrix} f_{j1}t^i & f_{j2}t^i & f_{j3}t^i \end{bmatrix}^{\mathrm{T}} \tag{13}$$

5.2 The rigorous model of spaceborne area array CCD images

Because the precision of the lunar control network ULCN2005 is described from several hundreds to 3 km, the precision of the backward resection might be reduced by control points of low precision and numerical insufficiency. Theories and experiments show that the result error is very large if control points are only used in calculating exterior orientation elements. For Clementine images providing orbit information of imaging time and photographed approximate vertically, orbit and attitude parameters and its correction model parameters can be served as observed values or virtual observed values in error equations in order to improve stability and reliability of unknown parameters solving. In this experiment, interpolation satellite position coordinates from fitting orbit are served as initial values, and the weight is calculated as the precision in 3 km. 0 is taken as the initial value in all attitudes, and the weight is calculated as the precision of 1°, which is the same as ULCN2005 calculation (Brent *et al*., 2006).

When Eq. (10) is adopted as basal error equation, the adjustment model is:

$$\begin{cases} \boldsymbol{V}_x = \boldsymbol{B}_X \boldsymbol{X}_X + \boldsymbol{B}_L \boldsymbol{X}_L + \boldsymbol{B}_A \boldsymbol{X}_A + \boldsymbol{B}_I \boldsymbol{X}_I - \boldsymbol{L}_x ... \boldsymbol{P}_x \\ \boldsymbol{V}_X = \boldsymbol{E}\boldsymbol{X}_X - \boldsymbol{L}_X ... \boldsymbol{P}_X \\ \boldsymbol{V}_L = \boldsymbol{E}\boldsymbol{X}_L + \boldsymbol{B}_a \boldsymbol{X}_a - \boldsymbol{L}_L ... \boldsymbol{P}_L \\ \boldsymbol{V}_A = \boldsymbol{E}\boldsymbol{X}_A - \boldsymbol{L}_A ... \boldsymbol{P}_A \\ \boldsymbol{V}_I = \boldsymbol{E}\boldsymbol{X}_I - \boldsymbol{L}_I ... \boldsymbol{P}_I \end{cases} \quad (14)$$

When Eq. (11) is adopted as basal error equation, the adjustment model is:

$$\begin{cases} \boldsymbol{V}_x = \boldsymbol{B}_X \boldsymbol{X}_X + \boldsymbol{B}_a \boldsymbol{X}_a + \boldsymbol{B}_A \boldsymbol{X}_A + \boldsymbol{B}_I \boldsymbol{X}_I - \boldsymbol{L}_x ... \boldsymbol{P}_x \\ \boldsymbol{V}_X = \boldsymbol{E}\boldsymbol{X}_X - \boldsymbol{L}_X ... \boldsymbol{P}_X \\ \boldsymbol{V}_a = \boldsymbol{E}\boldsymbol{X}_a - \boldsymbol{L}_a ... \boldsymbol{P}_a \\ \boldsymbol{V}_A = \boldsymbol{E}\boldsymbol{X}_A - \boldsymbol{L}_A ... \boldsymbol{P}_A \\ \boldsymbol{V}_I = \boldsymbol{E}\boldsymbol{X}_I - \boldsymbol{L}_I ... \boldsymbol{P}_I \end{cases} \quad (15)$$

In Eq. (14) and Eq. (15), $\boldsymbol{V}$ is the correction vector of the observed data. Eq. (11)—Eq. (15) stand for error equations of observed values of the image point coordinate, measured values of the control points, observed values of the satellite position or the virtual observed values of its correction model parameters, observed values of attitudes, and measured values of interior elements respectively. $\boldsymbol{B}$ stands for the coefficient matrix, $\boldsymbol{X}$ stands for increment unknowns, and their suffix *X*, *L*, *A*, *I* and *a* indicate the coefficients or increment unknowns associated with coordinates of ground points, satellite orbits, attitudes, interior elements, orbit correction model parameters respectively. $\boldsymbol{L}$ stands for constants of error equation and $\boldsymbol{P}$ stands for the weight matrix.

6 EXPERIMENTS

In this study, 60 views of Clementine images in 10 strips are adopted as the data source, ranging from 68.5° S to 54.5° S, from 106.5° W to 171.0° W of the meridian with an area of about 195000km^2 near south pole of the Moon (Fig. 6). The optical sensor CCD matrix is 384×288, with the focal length f_0=0.09 m, and the general resolving power of the test images is about 450m. The control point networks of the Moon mainly include: ULCN1994, CLCN1997, ULCN2004, LOLCN2004 and ULCN2005. ULCN2005 is the highest one with the accuracy ranging 100—3000 m. ULCN2005 includes 272931 GCPs (Brent *et al*., 2006), within which 1261 GCPs have been surveyed in the Clementine images. Based on these GCPs and newly surveyed points, 400 ground point coordinates are contained in the testing images, of which 350 points are taken as control points and 50 points as check points (the black points in Fig. 6) evenly distributed in the area covered by images. Since the studied area is located in the South Pole area, the weight of control points has been computed based on its accuracy of 800 m.

Two different methods for orbit correction models have been utilized in this study, that is, each view of image has one set of independent constant correction parameters for orbit, each strip has one set of linear correction parameters for orbit (with the error Eq. (10) and Eq. (11) adopted separately). The lunar ground control points have also been processed with two methods as true values and observed value separately for adjustment. The interior orientation parameters have been taken as unknowns for all tests. The coordinate values of control points and check points are able to be obtained on the basis of corrected orientation parameters after adjustment. Compared with known values of these points, the statistic chart of mean square error M_X, M_Y, M_Z in *X*, *Y*, *Z* axis directions and M_{XYZ} (Table 1) is able to be achieved.

Two other tests have been carried out for comparison.

(1) Only the constant parameters of orbit correction model is taken as adjustment unknown parameters, the correction constant adopted separately is the increment unknown of SOCS and flight coordinate, and the MSE of check points are: M_X=730 m, M_Y=835 m, M_Z=4960 m; M_X=694 m, M_Y=732 m, M_Z=4422 m. It is shown that the accuracy of orbit system correction carried out in the flight coordinate is higher than that in SOCS.

(2) On the basis of TM projection coordinate in commercial software ERDAS LPS, the test of bundle adjustment (6 unknown parameters per scene) has been carried out, the accuracy of check points from different combinations is lower and the MSE difference between control points and check points is larger than the results in Table 1. It is shown that both the accuracy and reliability of bundle adjustment are improved in SOCS.

Having obtained high-accuracy orientation parameters, it is easy to acquire DOM and DEM data from the image matching processes. DEM and DOM images from the 3rd party software are shown in Fig. 7, and the processes include image matching, DEM extracting according to matching points and orientation parameters, orthorectification, mosaic, etc. TM projection is adopted in DOM and DEM making.

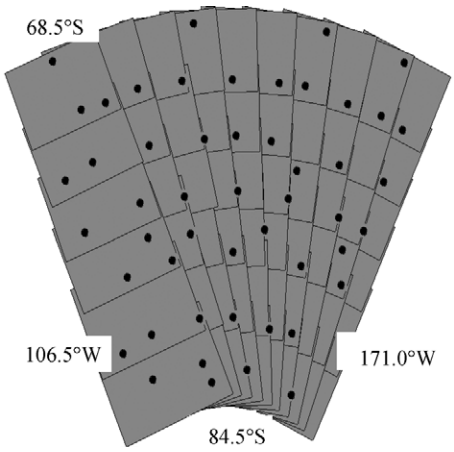

Fig. 6 Image covering and check points distribution

Table 1 Testing accuracy from Clementine image orientation

Test ways RMS	GCPs as true value		GCPs as observed value	
	MSE_GCP/m	MSE_CP/m	MSE_GCP/m	MSE_CP/m
Each image has one set of orbit parameters	M_{XYZ}=1355 M_X=209 M_Y=237 M_Z=1318	M_{XYZ}=1389 M_X=220 M_Y=234 M_Z=1351	M_{XYZ}=929 M_X=131 M_Y=133 M_Z=910	M_{XYZ}=1192 M_X=213 M_Y=263 M_Z=1142
Each strip has one set of orbit parameters	M_{XYZ}=1381 M_X=207 M_Y=214 M_Z=1349	M_{XYZ}=1424 M_X=202 M_Y=253 M_Z=1387	M_{XYZ}=951 M_X=121 M_Y=136 M_Z=933	M_{XYZ}=1203 M_X=217 M_Y=256 M_Z=1156

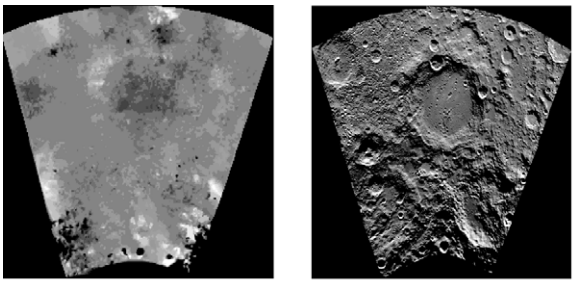

Fig. 7 Mosaic map for DEM and DOM

7 CONCLUSIONS

The following conclusions might be reached based on this study:

(1) The lunar curvature is not required to be taken into account when bundle adjustment is carried out in the Selenocentric Coordinate System, and the orbit segmentation is able to fit the combined adjustment between lunar images and other observation data.

(2) For Chang'e-1 images, if the accuracy of orbit surveying, or after adjustment, could reach 300m, the maximum positioning error would be less than 15m after the compensation of other orientation parameters.

(3) Due to the low accuracy, lunar control points can be taken into the error equation as weighted observed value and unknowns parameters to improve the accuracy of image orientation.

(4) The accuracy of orbit and attitude surveying on the Moon is much lower than that on the Earth, and the reliability of orientation parameters is able to be enhanced if the orbit and attitude data are taken as weighted observed value during adjustment computation with control points of lower accuracy and numerical deficiency.

(5) Instead of one bunch of modification parameters per scene, the same modification parameters are adopted in the flight coordinate for strip images, thus reducing the number of orientation parameters and the correlation of parameters, but the difference of orientation accuracy is smaller. It is significant for CE-1 linear array image with combined adjustment model in a large area of the Moon.

Since topographic mapping on the Moon based on remote sensing images has been taken as one important task in the next five-year plan of the State Bureau of Surveying and Mapping (RCMSD, 2008), the research on high accuracy lunar topographic mapping is significantly important to the Moon exploration.

REFERENCES

Archinal B A, Rosiek M R.,Kirk R L and Redding B L. 2006. The Unified Lunar Control Network 2005 (Open-File Report 2006-1367-Version1.0). http://pubs.usgs.gov/of/2006/ 1367(2008-05-03)

Giannone F. 2006. A Rigorous Model for High Resolution Satellite Imagery Orientation. Rome: University of Rome "La Sapienza" Faculty of Engineering

Kratky V. 1989. Rigorous photogrammetric processing of SPOT images at CCM Canada. *ISPRS Journal of Photogrammetry and Remote Sensing*, **44**: 53—71

Research Center of Surveying and Mapping Development.2008. Plan for Surveying and Mapping Technology for the Coming 11th Five Years. http://fazhan.sbsm.gov.cn/article//wxzy/200805/20080500034952. shtml (2008-11-03)

Wang R X. 2008a. EFP bundle triangulation using lunar imagery obtained from satellite three-line-array camera. *Science of Surveying and Mapping*, **33**(4): 5—7

Wang R X. 2008b.The interior accuracy estimation in the photogrammetric calculation of the stereoscopic imagery of The Chang'e-1. *Science of Surveying and Mapping*, **33**(2): 5—6,14

Wang Z Z. 1979. Principles of Photogrammetry. Beijing: Publishing House of Surveying and Mapping Beijing

Yuan X X and Zhang G. 2003. Object location of satellite imagery under lacking ground control points. *Geomatics and Information Science of Wuhan University*. **28**(5): 505—509

Zhang Y, Wang T, Zhu S L and Zhu B S. 2004. Application of combined ridge-stein estimator to linear pushbroom imagery exterior orientation. *Journal of Wuhan University*, **29**(10): 893—896.

Zhou Z M, Yi J J and Zhou Q. 1997. Principle and Application of GPS Surveying. Beijing: Publishing House of Surveying and Mapping

月球遥感影像高精度定位研究

张继贤[1], 邓喀中[2], 程春泉[1,2], 燕 琴[1], 宁晓刚[1], 郭 健[1]

1. 中国测绘科学研究院 对地观测技术国家测绘局重点实验室, 北京 100830;
2. 中国矿业大学 环测学院, 江苏 徐州 221116

摘 要: 高精度影像立体定位是月球地形测绘的基础。对嫦娥 1 号光学传感器方位元素误差和方位元素相关性对影像定位影响进行了仿真, 并建立了适合稀少、低精度控制点条件下月球光学影像区域网平差模型。该模型通过在月心直角坐标系(SOCS)进行影像空中三角测量来消除月球曲率引起的误差和测图范围限制, 通过轨道形状的拟合与插值来减小摄影时刻轨道位置的偶然误差, 在飞行坐标系中建立轨道修正模型来减少定向参数的数目, 对轨道和姿态增加约束条件来提高月面控制点数目稀少及精度低条件下外方位解算的精度与可靠性。文中以克莱门汀 10 条轨道 60 景约 195000 km^2 月球南极区面阵影像和 ULCN2005 控制网为数据源, 进行了不同方案的平差试验。通过对仿真和试验结果分析, 得出月球遥感影像定位部分有益的结论。

关键词: 严密模型, 影像定位, 月球测绘, 误差模拟

中图分类号: P236 文献标识码: A

引用格式: 张继贤, 邓喀中, 程春泉, 燕 琴, 宁晓刚, 郭 健. 2010. 月球遥感影像高精度定位研究. 遥感学报, **14**(3): 423—436

Zhang J X, Deng K Z, Cheng C Q, Yan Q, Ning X G and Guo J. 2010. Study on high-accuracy orientation with lunar remote sensing imagery. *Journal of Remote Sensing*. **14**(3): 423—436

1 引 言

月球是距离地球最近的天然卫星, 近年来各国的探月计划相继实施, 又一次掀起了探月高潮。中国于 2007 年发射了第一颗探月卫星——嫦娥 1 号(CE-1), 测绘月面地形是其首要任务之一。月面地形测绘为后续探月活动提供不可缺少的基础信息。光学影像是目前月面地形图测绘的主要数据源, 影像的匹配和影像的高精度定位仍然是月球光学影像测图的关键和核心。

月球的赤道半径是 1737.4 km, 约为地球半径的 3/11, 月球自身的几何形状及地形特征决定了月球影像的测图与地球有很大不同。目前, 商业航天遥感影像测图软件大多默认以地球卫星遥感影像为测图数据源, 将地球参数固化在系统中, 不能或仅以局部切面直角坐标系或地图投影坐标系中处理小范围月球影像。随着嫦娥 1 号遥感卫星任务的顺利完成, 月球影像高精度三维测图研究和生产任务已摆在中国测绘工作者面前。王任享院士对 CE-1 光学传感器摄影测量内部精度(2008b)和 1/4 轨道长条带影像空中三角测量进行了分析试验(2008a), 但总体来说, 中国对月球影像定位具体方法研究和试验的文献还很稀少。

2 月心直角坐标系光学影像共线方程

小范围内航空摄影测量常将地面摄影测量物方坐标系建立在地(月)球切面直角坐标系上或对应的投影平面为基础的直角坐标系上。由于地(月)球曲率的影响, 在球面切面直角坐标系中进行摄影测量处理时, 随着航线加长, 摄站 X_s 和 Z_s 以及倾角在数值甚至符号上均有变化, 因而将航线按适当长度分段并逐段按切面坐标系进行平差, 是摄影测量常用的方法(王任享, 2008a; 王之卓, 1979)。将三维月面空

收稿日期: 2009-02-24; 修订日期: 2009-04-01

基金项目: 国家自然科学基金(编号: 40871167, 40801192)。

第一作者简介: 张继贤(1965—), 男, 陕西商州人。教授, 博士生导师。主要研究方向为摄影测量与遥感、地理信息系统、3S 集成与应用。

通讯作者: E-mail: zhangjx@casm.ac.cn。

间转换到投影平面时存在变形，月球半径比地球小很多，其投影形变比地球更明显。本文试验数据影像范围内，即使切面直角坐标系原点或投影中心放在摄区中心部位，边缘影像距切面或投影面的距离也超过 25 km。对于地球遥感影像，由于在地心直角系下进行多源数据的联合处理可以减少数据在不同坐标系间的转换、适合大范围影像联合处理等优点，航天影像空中三角测量已逐渐过渡到地心直角坐标系下进行，线阵传感器影像定位模型主要形式如公式(1)(Kratky, 1989; 袁修孝, 2003)。

$$\begin{bmatrix} x \\ 0 \\ -f \end{bmatrix} = \lambda \boldsymbol{M}^{-1} \begin{bmatrix} X - X_s \\ Y - Y_s \\ Z - Z_s \end{bmatrix} \tag{1}$$

x 为像点对应像平面坐标系中 X 轴方向坐标； f 为焦距; X_s, Y_s, Z_s, X, Y, Z 分别为卫星摄影投影中心和地面点的地心直角坐标系坐标，$\boldsymbol{M}$ 为姿态与轨道参数相关旋转矩阵。

与地心直角坐标系中航天遥感影像空中三角测量类似，本文月球遥感影像的空中三角测量也在月心直角坐标系中进行，并采用与地球卫星遥感影像相似的定位模型。令:

$\boldsymbol{M} = \boldsymbol{R}_o^{\ E} \cdot \boldsymbol{R}_b^{\ o} \cdot \boldsymbol{R}_c^{\ b} = [m_{ij}]$, i,j=1,2,3。m_{ij} 为矩阵元素。式中，$\boldsymbol{R}_o^{\ E}$, $\boldsymbol{R}_b^{\ o}$, $\boldsymbol{R}_c^{\ b}$ 分别为轨道坐标系到月心直角坐标系、卫星本体坐标系到轨道坐标系、传感器坐标系到卫星本体坐标系的转换，他们分别是卫星状态矢量、姿态、传感器安置角的函数。

本文区域网平差试验数据为面阵传感器影像，式(1)中左边$[x,\ 0,\ -f]^{\mathrm{T}}$ 相应变为$[x-x_0,\ y-y_0,\ -f]^{\mathrm{T}}$，可得地心直角坐标系共线方程表达式:

$$\begin{cases} x - x_0 = -f \dfrac{m_{11}(X - X_s) + m_{21}(Y - Y_s) + m_{31}(Z - Z_s)}{m_{13}(X - X_s) + m_{23}(Y - Y_s) + m_{33}(Z - Z_s)} \\ y - y_0 = -f \dfrac{m_{12}(X - X_s) + m_{22}(Y - Y_s) + m_{32}(Z - Z_s)}{m_{13}(X - X_s) + m_{23}(Y - Y_s) + m_{33}(Z - Z_s)} \end{cases} \tag{2}$$

由于轨道坐标系到月心直角坐标系的转换矩阵是卫星状态矢量的函数，平差迭代过程中，其精度随轨道的逐步精化而提高。传感器坐标系到本体坐标系的转换矩阵由仪器检校参数得出，其精度一般较高，且与外方位元素相关性强，其对定位的影响可通过合并强相关项的方法来减小。因此平差未知数可选择影像的内、外方位元素和月面点坐标增量，其线性化后误差方程式的一般形式为(王之卓, 1979):

$$\begin{cases} v_x = (x) - x + f_{11}\Delta X_s + f_{12}\Delta Y_s + f_{13}\Delta Z_s + \\ \quad f_{14}\Delta\omega + f_{15}\Delta\varphi + f_{16}\Delta\kappa + f_{17}\Delta f + \\ \quad f_{18}\Delta x_0 - f_{11}\Delta X - f_{12}\Delta Y - f_{13}\Delta Z \\ v_y = (y) - y + f_{21}\Delta X_s + f_{22}\Delta Y_s + f_{23}\Delta Z_s + \\ \quad f_{24}\Delta\omega + f_{25}\Delta\varphi + f_{26}\Delta\kappa + f_{27}\Delta f + \\ \quad f_{29}\Delta y_0 - f_{21}\Delta X - f_{22}\Delta Y - f_{23}\Delta Z \end{cases} \tag{3}$$

f_{ij}(i=1,2, j=1,2,…,8)为线性化后误差方程系数; (x), (y)为根据定向参数的地面点坐标的计算值; x, y 为像点坐标量测值。ΔX_s, ΔY_s, ΔZ_s, $\Delta\omega$, $\Delta\varphi$, $\Delta\kappa$为外方位元素改正值; Δx_0、Δy_0 为内方位元素改正值; ΔX, ΔY, ΔZ 为地面点改正值。

3 嫦娥 1 号卫星(CE-1)线阵影像定位误差模拟

影像定位误差的影响因素非常复杂，严密模型中要将所有的误差影响因素考虑是不可能也不现实的。没有被考虑的影响因素带来的定位误差，可以通过修正引入模型中的与其相关的参数补偿。同时，当定向参数中有相关性参数时，由于未知数间不是完全相关，相互补偿的同时给定位带来新的误差影响因素，给未知数解算的稳定性和可靠性带来负面影响。因此，遥感影像严密定位去相关性(张艳等, 2004)、以及相关性参数(如位置和姿态)通过测控或平差计算达到什么精度范围内，他们之间补偿的残差相对于定位需求精度可以忽略，也是研究月球影像定位模型需考虑的问题。本文以月球 CE-1 光学传感器为对象，运用仿真手段定量研究方位元素误差和方位元素相关性对影像定位误差的影响。

由于 CE-1 光学成像仪为线阵传感器，以获取影像某一行影像中心对应的月面点为原点、线阵方向为 X 轴，卫星飞行方向为 Y 轴正向的月球切面直角坐标系中，月面地形使用以下正弦函数模拟:

$$\begin{cases} Z = \mathrm{d}H \times \sin(2\pi X / Tt) + \sqrt{R_M^2 - X^2} - R_M \\ Y = 0 \end{cases} \tag{4}$$

式中, R_M 为月球半径, X 为影像对应地面点在线阵方向的坐标。

该函数以圆形月球形状为基础，以振幅为 dH=3 km 的正弦曲线叠加作为模拟地形，该模型在影像范围内，不同高度的地形在影像任意区域中能体现，地形形状见图 1。

嫦娥光学传感器相关参数: 焦距 f=23.33mm,其焦面 CCD 面阵为 1024×1024 像元，取左中右 3 线

构成前、正、后视 3 个线阵，线阵间视线夹角为 17°，截取的每条线阵含 512 像元，每个像元尺寸为 14 μm。轨道为近极轨道，设计高度为 200km(王任享，2008a)。

进行嫦娥卫星影像直接定位误差仿真时，卫星摄影中心 X_s, Y_s, Z_s 值各加 300m 作为误差；内方位元素 x_0, y_0, f_0 各加 0.05mm 作为误差；卫星姿态角 ω, φ, κ 各加入 0.1°作为误差；以式(2)、式(3)为基础，以模拟地形、CE-1 光学传感器参数和设计轨道设置摄影参数，以 CE-1 三线阵传感器下视和后视进行立体定位误差仿真，即以无误差的定向参数模拟成像，以有误差的定向参数与模拟影像进行前方交会立体定位，模拟摄影状态如图 2。得影像定位误差沿线阵方向 dX、沿卫星飞行方向 dY 以及高程方向 dZ 曲线如图 3，横轴 X 为一行影像对应地面点坐标。

从上述误差图可以看出，影像直接定位误差较大，误差大小与像元在线阵中排列位置基本成线性关系，与地形变化一致。

相关性元素误差补偿残差模拟以姿态、焦距作平差未知数参数，将其他带有误差的定向参数作为“真值”，以两个控制点置于线阵影像两端位置，以式(3)为基础，平差计算未知数修正值，并以平差值和带有误差的未平差参数值为定向数据进行定位，得一行影像定位误差沿线阵方向 dX、沿卫星飞行方向 dY 以及高程方向 dZ 曲线如图 4，横轴 X 仍为一行影像对应地面点坐标。

由于卫星平台的稳定性以及线阵影像不同行间为平行投影，控制点附近的影像行与控制点所在的影像行内外方位元素有相似的误差，它们直接定位误差和补偿后残差虽然受不同地形影响有所差异，但它们的规律是一样的，控制点置于不同影像行两端也有相似的结果。仿真结果表明，如果通过测控或平差计算，卫星位置精度达到 300 m 范围内，像

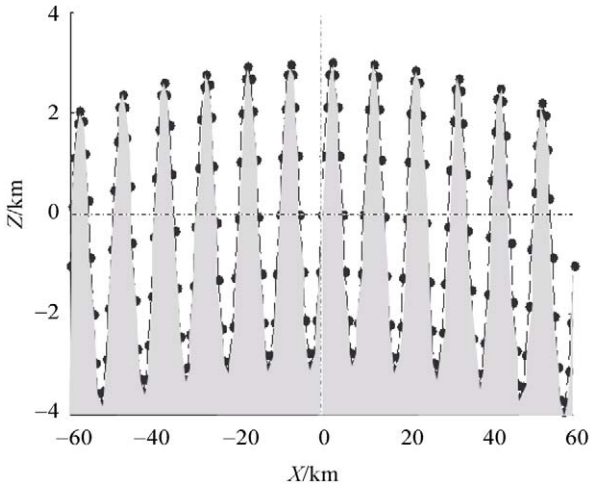

图 1 模拟地形

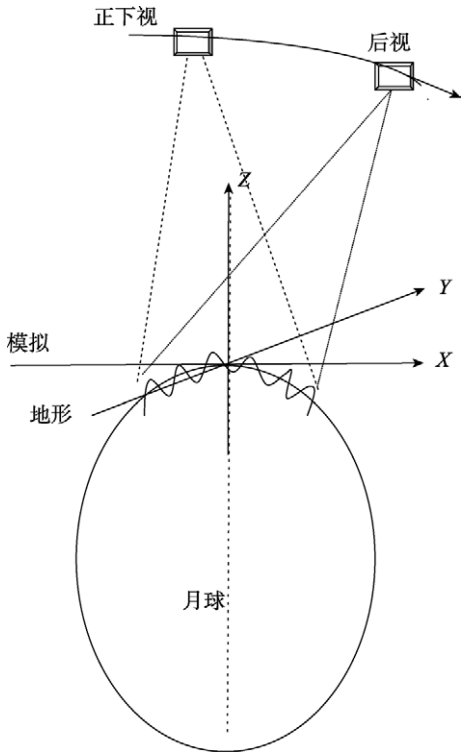

图 2 模拟线阵传感器立体摄影

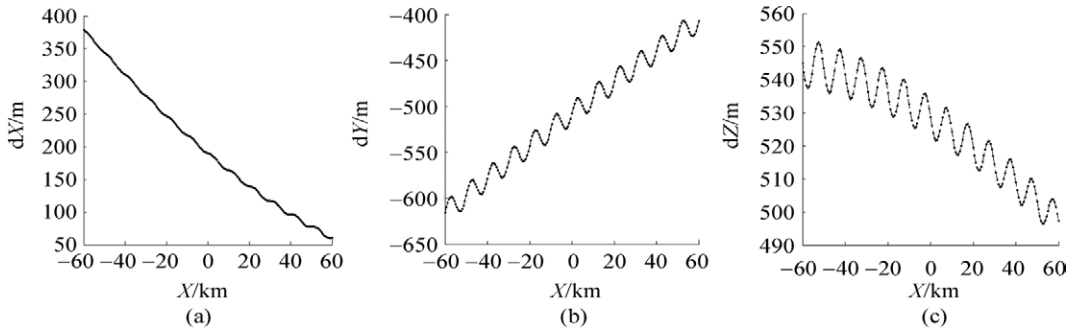

图 3 定位误差模拟

(a) X 轴; (b) Y 轴; (c) Z 轴

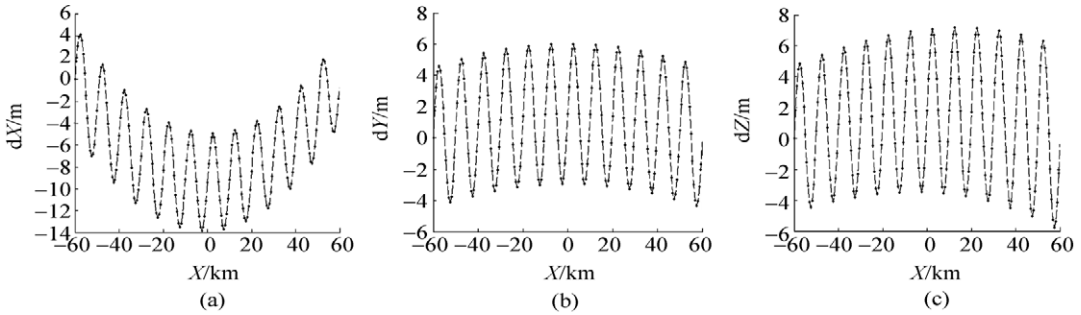

图 4 相关性元素补偿残差模拟
(a) X 轴; (b) Y 轴; (c) Z 轴

主点坐标检校精度优于 0.05 mm, 定位过程中将它们当作真值, 在以姿态和焦距作为未知数的情况下, 相对于控制点的高程起伏即使达到 3 km, 补偿后的残差三轴方向最大值均小于 15 m, 相对于月面控制点精度以及嫦娥影像分辨率, 是可以接受的。

4 轨道修正模型

将传感器位置修正模型建立在飞行坐标系上, 通过轨道参数的拟合与卫星位置插值来减少卫星测控星历的偶然误差, 通过月面控制点来减少卫星轨道的系统误差。

4.1 轨道形状的拟合与卫星位置的插值

轨道形状的拟合与插值是为了去除卫星摄影时刻位置的偶然误差, 使同一轨道段影像摄影时刻位置初值误差主要表现为系统性。影像的辅助数据提供非惯性坐标系卫星离散位置矢量, 根据这些位置即可拟合出卫星运行的轨道形状。由于月球自转影响, 首先将所有非惯性坐标系月球星历坐标转换到惯性月心直角坐标系下。设第 i 组数据星历时刻月固月心直角坐标系与惯性月心直角坐标系间的月球自转夹角 θ_i, 卫星位置值在两坐标系间的坐标转换关系有:

$$\begin{bmatrix} X_{iI} & Y_{iI} & Z_{iI} \end{bmatrix}^{\mathrm{T}} = \boldsymbol{R}_3(\theta_i)\begin{bmatrix} X_{iR} & Y_{iR} & Z_{iR} \end{bmatrix}^{\mathrm{T}} \quad (5)$$

$[X_{iR}\ Y_{iR}\ Z_{iR}]$为月固月心直角坐标系下的坐标, $[X_{iI}\ Y_{iI}\ Z_{iI}]$为惯性月心直角坐标系下的坐标。

在惯性坐标系下六轨道参数 a, e, i, Ω, ω, f 与三维坐标关系式:

$$\begin{cases} X_{iI} = r(\cos\Omega\cos u - \sin\Omega\sin u_i\cos i) \\ Y_{iI} = r(\sin\Omega\cos u + \cos\Omega\sin u_i\cos i) \\ Z_{iI} = r\sin u_i\sin i \end{cases} \quad (6)$$

式中, $r = \dfrac{a(1-\mathrm{e}^2)}{1+\mathrm{e}\cos f}$, $u_i = \omega + f_i$

以上两式为基础, 在提供若干时刻及相应卫星位置的情况下, 可以按最小二乘拟合出惯性地心直角坐标系中轨道参数, 拟合出的轨道参数进行任意时刻位置的插值和速度矢量的计算(Zhou 等, 1997)。

4.2 飞行坐标系及轨道修正模型

飞行坐标系以卫星飞行速度方向为 X 轴, Y 轴垂至于位置和速度向量构成的平面, Z 轴按右手规则确定, 如图 5 中 O_1-$X_1Y_1Z_1$ 中和 O_2-$X_2Y_2Z_2$。坐标系三轴在地心直角坐标系中的单位矢量数学定义表达式为:

$$\begin{cases} \boldsymbol{X}_v = [(X_v)_X, (X_v)_Y, (X_v)_Z] = \boldsymbol{V}(t)/\|\boldsymbol{V}(t)\| \\ \boldsymbol{Y}_v = [(Y_v)_X, (Y_v)_Y, (Y_v)_Z] = [\boldsymbol{P}(t)\times\boldsymbol{V}(t)]/\|\boldsymbol{P}(t)\times\boldsymbol{V}(t)\| \\ \boldsymbol{Z}_v = [(Z_v)_X, (Z_v)_Y, (Z_v)_Z] = \boldsymbol{X}_v\times\boldsymbol{Y}_v \end{cases} \quad (7)$$

式中, $\boldsymbol{P}(t_i)$, $\boldsymbol{V}(t_i)$ 为卫星在月心直角坐标系中的位置和速度矢量。

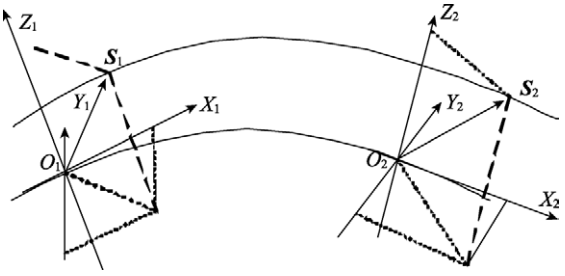

图 5 卫星轨道系统误差示意图

因此, 当卫星的位置为月固月心直角坐标系中的数值时, 飞行坐标系到月固月心直角系的转换矩为:

$$R_V E = \begin{bmatrix} (X_v)_X & (Y_v)_X & (Z_v)_X \\ (X_v)_Y & (Y_v)_Y & (Z_v)_Y \\ (X_v)_Z & (Y_v)_Z & (Z_v)_Z \end{bmatrix} \quad (8)$$

轨道修正模型在飞行坐标系三轴方向用线性函数或低阶多项式表达, 即:

$$\begin{cases}\Delta X_V = a_0 + a_1 t + \cdots \\ \Delta Y_V = b_0 + b_1 t + \cdots \\ \Delta Z_V = c_0 + c_1 t + \cdots\end{cases} \tag{9}$$

a_i, b_i, c_i(i=0,1,…, n)为多项式系数; t 为影像摄影时相对时刻。

虽然较短时间内一段卫星轨道在月心直角坐标系下需高阶多项式表达，但航天遥感卫星在一定的时间段内运行轨道相对稳定，轨道误差系统性明显。由于飞行坐标系随卫星在轨道上一起移动、旋转，轨道误差在飞行坐标系下的变化是很缓慢的，如一定时间段内轨道测控时间同步系统误差(真近点角、近地点角)是轨道误差主要影响因素(Giannone, 2006)，相应轨道误差投影到月心直角坐标系中三轴方向上均是变化的曲线，但在飞行坐标系中却近似表现为 X 轴方向上的一个常量，图 5 为移动的飞行坐标系 O_1-$X_1Y_1Z_1$ 和 O_2-$X_2Y_2Z_2$ 中摄站位置修正矢量 $\boldsymbol{O}_1\boldsymbol{S}_1$ 和 $\boldsymbol{O}_2\boldsymbol{S}_2$。误差曲线形式越简单，变化频率越低，用多项式拟合时，多项式阶数要求更低，定向参数个数更少，有利于在控制点数目少、精度低条件下提高定向参数求解的可靠性。

5 航天面阵影像定位严密模型

5.1 飞行坐标系摄站位置坐标增量未知数系数

式(3)中卫星位置误差方程系数 f_{11}, f_{12}, f_{13}, f_{21}, f_{22}, f_{23} 为月心直角坐标系下卫星位置未知数对应值，需将式(3)表达为含有飞行坐标系轨道修正模型参数的误差方程式，由于平差数据源为 Clementine 光学面阵传感器影像，根据平差未知数参数选择的不同，有如下 2 种误差方程式。

当每景影像一组外方位元素修正未知数时，误差方程为:

$$\begin{cases}v_x = (x) - x + f_{a01}\Delta X_{Vs} + f_{b01}\Delta Y_{Vs} + f_{c01}\Delta Z_{Vs} + \\ \quad f_{14}\Delta\omega + f_{15}\Delta\varphi + f_{16}\Delta\kappa + f_{17}\Delta f + \\ \quad f_{18}\Delta x_0 - f_{11}\Delta X - f_{12}\Delta Y - f_{13}\Delta Z \\ v_y = (y) - y + f_{a02}\Delta X_{Vs} + f_{b02}\Delta X_{Vs} + f_{c02}\Delta X_{Vs} + \\ \quad f_{24}\Delta\omega + f_{25}\Delta\varphi + f_{26}\Delta\kappa + f_{27}\Delta f + \\ \quad f_{29}\Delta y_0 - f_{21}\Delta X - f_{22}\Delta Y - f_{23}\Delta Z\end{cases} \tag{10}$$

式(10)中卫星位置增量未知数用式(9)表达。

当每条轨道段所有影像采用一组相同轨道修正模型参数、每景影像仍采用一组姿态增量参数作为未知数时，有误差方程:

$$\begin{cases}v_x = (x) - x + \sum_{i=0}^{n} f_{ai1}a_i + \sum_{i=0}^{n} f_{bi1}b_i + \sum_{i=0}^{n} f_{ci1}c_i + \\ \quad f_{14}\Delta\omega + f_{15}\Delta\varphi + f_{16}\Delta\kappa + f_{17}\Delta f + \\ \quad f_{18}\Delta x_0 - f_{11}\Delta X - f_{12}\Delta Y - f_{13}\Delta Z \\ v_y = (y) - y + \sum_{i=0}^{n} f_{ai2}a_i + \sum_{i=0}^{n} f_{bi2}b_i + \sum_{i=0}^{n} f_{ci2}c_i + \\ \quad f_{24}\Delta\omega + f_{25}\Delta\varphi + f_{26}\Delta\kappa + f_{27}\Delta f + \\ \quad f_{29}\Delta y_0 - f_{21}\Delta X - f_{22}\Delta Y - f_{23}\Delta Z\end{cases} \tag{11}$$

式(10)，式(11)中, f_{aij}, f_{bij}, f_{cij}(i=0,1,…; j=1,2，下同)为飞行坐标系轨道修正模型参数对应误差方程系数; (x), (y)为计算值; x, y 为像点坐标量测值。

由飞行坐标系的定义知，飞行坐标系与月心直角坐标系间的坐标转换有关系式:

$$\begin{bmatrix}X_s & Y_s & Z_s\end{bmatrix}^{\mathrm{T}} = \begin{bmatrix}X_{s0} & Y_{s0} & Z_{s0}\end{bmatrix}^{\mathrm{T}} + R_V E\begin{bmatrix}\Delta X_{Vs} & \Delta Y_{Vs} & \Delta Z_{Vs}\end{bmatrix}^{\mathrm{T}} \tag{12}$$

因此，式(11)飞行坐标系修正模型参数未知数系数与式(3)月心直角坐标系误差方程系数有关系式:

$$\begin{bmatrix}f_{aij} & f_{bij} & f_{cij}\end{bmatrix}^{\mathrm{T}} = R^T{}_v E\begin{bmatrix}f_{j1}t^i & f_{j2}t^i & f_{j3}t^i\end{bmatrix}^{\mathrm{T}} \tag{13}$$

5.2 航天面阵影像严密模型

由于月球控制网 ULCN2005 精度在几百米到 3 km 间，数目较少且精度较差的控制点给航天摄影后方交会解算精度带来了不利的影响。理论和试验均表明，单纯依靠月面控制点求解定向参数误差很大。由于试验用克莱门汀影像提供了部分卫星摄影时的轨道信息，且为近似竖直摄影,为了减小控制点精度低和数目较少给方位元素求解稳定性和可靠性带来的不利影响，将卫星轨道和姿态当作带权观测值，或其修正模型参数当作带权虚拟观测值引入误差方程组。试验中传感器位置以提供的辅助数据拟合轨道插值位置为初值、精度按 3 km 进行权值计算，相机指向角初值按 0°计算，与 ULCN2005 计算时使用的精度相同，按 1°进行权值计算(Brent 等, 2006)。

误差方程采用式(10)时，使用的平差模型为:

$$\begin{cases}\boldsymbol{V}_x = \boldsymbol{B}_X\boldsymbol{X}_X + \boldsymbol{B}_L\boldsymbol{X}_L + \boldsymbol{B}_A\boldsymbol{X}_A + \boldsymbol{B}_I\boldsymbol{X}_I - \boldsymbol{L}_x \cdots \boldsymbol{P}_x \\ \boldsymbol{V}_X = \boldsymbol{E}\boldsymbol{X}_X - \boldsymbol{L}_X \cdots \boldsymbol{P}_X \\ \boldsymbol{V}_L = \boldsymbol{E}\boldsymbol{X}_L + \boldsymbol{B}_a\boldsymbol{X}_a - \boldsymbol{L}_L \cdots \boldsymbol{P}_L \\ \boldsymbol{V}_A = \boldsymbol{E}\boldsymbol{X}_A - \boldsymbol{L}_A \cdots \boldsymbol{P}_A \\ \boldsymbol{V}_I = \boldsymbol{E}\boldsymbol{X}_I - \boldsymbol{L}_I \cdots \boldsymbol{P}_I\end{cases} \tag{14}$$

误差方程采用式(11)时，使用的平差模型为:

$$\begin{cases} \boldsymbol{V}_x = \boldsymbol{B}_X \boldsymbol{X}_X + \boldsymbol{B}_a \boldsymbol{X}_a + \boldsymbol{B}_A \boldsymbol{X}_A + \boldsymbol{B}_I \boldsymbol{X}_I - \boldsymbol{L}_x \cdots \boldsymbol{P}_x \\ \boldsymbol{V}_X = \boldsymbol{E}\boldsymbol{X}_X - \boldsymbol{L}_X \cdots \boldsymbol{P}_X \\ \boldsymbol{V}_a = \boldsymbol{E}\boldsymbol{X}_a - \boldsymbol{L}_a \cdots \boldsymbol{P}_a \\ \boldsymbol{V}_A = \boldsymbol{E}\boldsymbol{X}_A - \boldsymbol{L}_A \cdots \boldsymbol{P}_A \\ \boldsymbol{V}_I = \boldsymbol{E}\boldsymbol{X}_I - \boldsymbol{L}_I \cdots \boldsymbol{P}_I \end{cases} \quad (15)$$

式(14)、式(15)中, $\boldsymbol{V}$ 代表观测值改正向量;式(11)—式(15)分别代表像点坐标观测值、控制点坐标测量值、卫星摄影时位置观测值($\boldsymbol{V}_L$)或其修正模型参数虚拟观测值($\boldsymbol{V}_a$)、姿态角观测值以及内方位元素测量值误差方程式。$\boldsymbol{B}$ 代表系数矩阵; $\boldsymbol{X}$ 代表未知数; 其下标 X, L, A, I, a 分别代表地面点坐标增量、卫星摄影时位置观测值增量、姿态观测值增量、内方位元素观测值增量、轨道修正模型参数等相关的参数。$\boldsymbol{L}$ 代表误差方程常数项, $\boldsymbol{P}$ 代表权阵。

6 克莱门汀影像试验

以克莱门汀影像为试验数据, 影像覆盖范围为 68.5°S—54.5°S, 106.5°W—171.0°W 的扇形区域(图 6), 共 10 轨道 60 景影像, 覆盖面积约为 195000 km^2。该影像光学传感器为 384×288 大小面阵传感器, 相机焦距 f_0=0.09 m, 试验区影像平均分辨率约为 450m。目前已有的月球控制网主要有 5 种, 即: ULCN1994, CLCN1997, ULCN2004, LOL-CN2004 和 ULCN2005, 其中 ULCN2005 精度最高, 达到 100—3000 m, 控制点数目达到 272931 个(Brent 等, 2006), 其中 1261 个点已经在克莱门汀影像上进行了量测。本文以影像覆盖区已有量测点为基础, 加上一些补测点, 共获取了 400 对影像点地理坐标, 350 个用作本次试验的控制点, 50 个用作检查点(图 6 中黑点), 较均匀分布在测图区域。由于影像分布在南极区, 控制点权值按精度为 800m 进行计算确定。

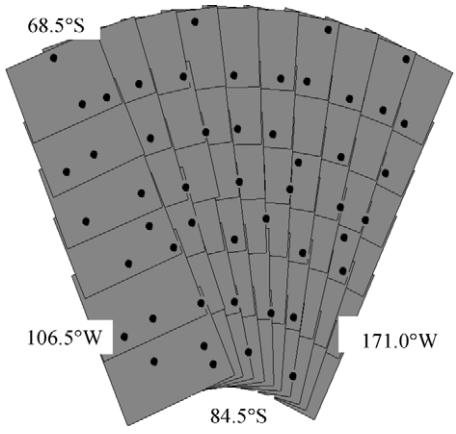

图 6 影像覆盖范围及检查点分布

对卫星的轨道修正模型采用两种不同的方法进行试验, 分别是: 每景影像一组独立常数修正参数, 每条轨道条带影像一组线性修正参数(分别采用式(10)和式(11)中的误差方程); 对月面控制点也按两种方案进行处理, 即按真值进行平差和按观测值进行平差。所有试验内方位元素均作为未知数参加平差。以平差后的定向参数值为基础即可获得控制点和检查点像点的前方交会值, 与已知值(控制点参加平差时采用平差值)进行比较, 得到月心直角坐标系中 X, Y, Z 三方向统计中误差 M_X, M_Y, M_Z 以及综合中误差 M_{XYZ} 见表 1。

表 **1** 克莱门汀影像定位试验精度统计

平差方法 中误差	控制点作真值 平差精度		控制点作观测值 平差精度	
	GCPs/m	CPs/m	GCPs/m	CPs/m
每景影像 一组位置 未知数	M_{XYZ}=1355 M_X=209 M_Y=237 M_Z=1318	M_{XYZ}=1389 M_X=220 M_Y=234 M_Z=1351	M_{XYZ}=929 M_X=131 M_Y=133 M_Z=910	M_{XYZ}=1192 M_X=213 M_Y=263 M_Z=1142
每段轨道 一组位置 未知数	M_{XYZ}=1381 M_X=207 M_Y=214 M_Z=1349	M_{XYZ}=1424 M_X=202 M_Y=253 M_Z=1387	M_{XYZ}=951 M_X=121 M_Y=136 M_Z=933	M_{XYZ}=1203 M_X=217 M_Y=256 M_Z=1156

为了比较, 我们还进行了另外两组试验:

(1) 仅轨道修正模型常量参数作为平差未知数, 其他参数均作为已知值, 但修正常量分别为月心直角坐标系和飞行坐标系中的增量未知数, 平差后检查点中误差分别为: M_X=730m, M_Y=835m, M_Z=4960 m; M_X=694m, M_Y=732m, M_Z=4422m。表明在飞行直角坐标系中进行轨道系统修正比月心直角坐标系中进行轨道系统校正精度有一定优势, 这种优势从理论上容易得出轨道跨度越大、系统误差越大表现越明显。

(2) 同样的数据在商业软件 ERDAR LPS 中以 TM 投影坐标系为基础进行了区域网平差试验(每景影像一组定向参数), 本文不同组合试验检查点精度均高于投影坐标系中的试验结果, 且控制点和检查点中误差差异明显要小, 表明区域网平差精度与可靠性均有提高。

获得高精度定向参数后, 通过影像间的匹配, 很容易获取 DOM 和 DEM 数据。图(7)为通过第三方软件得到的 DEM 和 DOM 影像, 所经历的后继工序包括影像间的匹配、根据匹配点和定向参数前方交会 DEM 提取、根据定向参数和 DEM 进行正射纠正、拼接等, 平面成像采用横轴墨卡托(TM)投影。

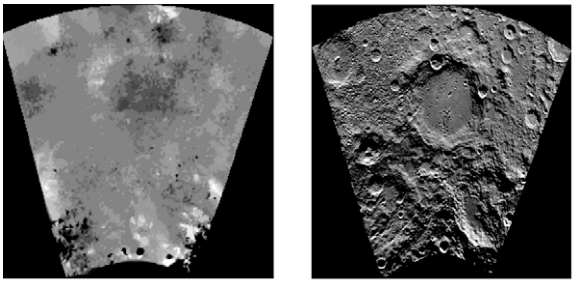

图 7 DEM 及 DOM 拼接图

7 结 论

从以上的理论分析和试验中可以得出如下结论:

(1) 月心直角坐标系下进行空中三角测量不用考虑月球曲率的影响, 通过适当的轨道分段处理能够适应全月球影像与其他观测数据的统一平差;

(2) 对于嫦娥月球卫星影像, 轨道测控或平差后的精度达到 300m, 通过修正其他定向参数对定位误差进行补偿, 其带来的最大定位误差小于 15m;

(3) 由于月面控制点精度较低, 将月面控制点作为带权观测值引入误差方程, 对提高影像定位精度有一定的作用;

(4) 月球卫星轨道和姿态测控精度远比地球卫星低, 在平差中将轨道和姿态作为带权观测值引入误差方程, 对控制点数目少且精度低情况下定向参数解算的稳定可靠性起着很重要的作用;

(5) 较长一段轨道上的影像, 通过在飞行坐标系上使用一组相同的修正参数代替每景影像一组修正参数, 实现了定向参数个数的大幅减少、线元素与角元素相关性的降低, 而定位精度差异不大, 这对 CE-1 线阵影像定位、对大范围影像定向参数同时平差求解, 均有一定的参考价值。

国家测绘局将月球遥感测图作为下一个五年规划内容之一(RCMSD, 2008), 而实现月球高精度地形测绘, 与地球相比有非常大的区别, 前期对其关键技术进行探讨与研究, 无论对该计划的顺利实施以及后继探月活动, 均起着十分重要的作用。

REFERENCES

Archinal B A, Rosiek M R.,Kirk R L and Redding B L. 2006. The Unified Lunar Control Network 2005 (Open-File Report 2006-1367-Version1.0). http://pubs.usgs.gov/of/2006/ 1367(2008-05-03)

Giannone F. 2006. A Rigorous Model for High Resolution Satellite Imagery Orientation. Rome: University of Rome “La Sapienza” Faculty of Engineering

Kratky V. 1989. Rigorous photogrammetric processing of SPOT images at CCM Canada. *ISPRS Journal of Photogrammetry and Remote Sensing*, **44**: 53—71

Research Center of Surveying and Mapping Development.2008. Plan for Surveying and Mapping Technology for the Coming 11th Five Years. http://fazhan.sbsm.gov.cn/article//wxzy/200805/20080500034952. shtml (2008-11-03)

Wang R X. 2008a. EFP bundle triangulation using lunar imagery obtained from satellite three-line-array camera.*Science of Surveying and Mapping*, **33**(4): 5—7

Wang R X. 2008b.The interior accuracy estimation in the photogrammetric calculation of the stereoscopic imagery of The Chang’e-1. *Science of Surveying and Mapping*, **33**(2): 5—6,14

Wang Z Z. 1979.Principles of Photogrammetry. Beijing: Publishing House of Surveying and Mapping Beijing

Yuan X X and Zhang G. 2003.Object location of satellite imagery under lacking ground control points. *Geomatics and Information Science of Wuhan University*. **28**(5): 505—509

Zhang Y, Wang T, Zhu S L and Zhu B S. 2004.Application of combined ridge-stein estimator to linear pushbroom imagery exterior orientation. *Journal of Wuhan University*, **29**(10): 893—896.

Zhou Z M, Yi J J and Zhou Q. 1997. Principle and Application of GPS Surveying. Beijing: Publishing House of Surveying and Mapping

附中文参考文献

国家测绘局测绘发展研究中心. 2008.测绘科技发展“十一五”规划. http://fazhan.sbsm.gov.cn/article//wxzy/200805/20080500034952. shtml(2008-11-03)

王任享. 2008a.月球卫星三线阵CCD影像EFP光束法空中三角测量, 测绘科学, **33**(4): 5—7

王任享. 2008b.嫦娥一号立体影像的摄影测量内部精度估算. 测绘科学, **33**(2): 5—6,14

王之卓. 1979.摄影测量原理. 北京: 测绘出版社

袁修孝, 张过. 2003.缺少控制点的卫星遥感对地目标定位. 武汉大学学报(信息科学版), **28**(5): 505—509

张艳, 王涛, 朱述龙, 朱宝山. 2004.岭压缩组合估计在线阵推扫式影像外定向中的应用. 武汉大学学报(信息科学版), **29**(10): 893—896

周忠谟, 易杰军, 周琪. 1997.GPS 卫星测量原理与应用. 北京: 测绘出版社